Comput Mech (2013) 51:187–201
DOI 10.1007/s00466-012-0716-8

ORIGINAL PAPER

A two-way coupled multiscale model for predicting damage-associated performance of asphaltic roadways

Yong-Rak Kim · Flavio V. Souza · Jamilla Emi Sudo Lutif Teixeira

Received: 7 October 2011 / Accepted: 15 April 2012 / Published online: 1 May 2012

Abstract This paper presents a quasi-static multiscale computational model with its verification and rational applications to mechanical behavior predictions of asphaltic roadways that are subject to viscoelastic deformation and fracture damage. The multiscale model is based on continuum thermomechanics and is implemented using a finite element formulation. Two length scales (global and local) are two-way coupled in the model framework by linking a homogenized global scale to a heterogeneous local scale representative volume element. With the unique multiscaling and the use of the finite element technique, it is possible to take into account the effect of material heterogeneity, viscoelasticity, and anisotropic damage accumulation in the small scale on the overall performance of larger scale structures. Along with the theoretical model formulation, two example problems are shown: one to verify the model and its computational benefits through comparisons with analytical solutions and single-scale simulation results, and the other to demonstrate the applicability of the approach to model general roadway structures where material viscoelasticity and cohesive zone fracture are involved.

Y.-R. Kim (✉)
Department of Civil Engineering, Kyung Hee University,
224 Engineering Building, Yongin-si,
Gyeonggi-do 446-701, South Korea
e-mail: ykim3@khu.ac.kr

F. V. Souza
Multimech Research and Development, LLC, Omaha, NE 68022,
USA
e-mail: fsouza@multimechrd.com

J. E. S. L. Teixeira
Centro Tecnológico, Departamento de Engenharia Civil (CT-DEC),
Universidade Federal do Espírito Santo (UFES), Av. Fernando Ferrari,
514, CT I, Goiabeiras, Vitoria, ES 29060-970, Brazil
e-mail: jamilla.teixeira@ufes.br

Keywords Multiscale modeling · Asphalt pavement · Viscoelasticity · Fracture · Cohesive zone · Finite element method

1 Introduction

Approximately 96 % of all paved roads and streets in the US, almost two million miles, are surfaced with asphalt concrete mixtures. On the average, the asphalt concrete industry produces and places approximately 500 million tons of asphalt mixtures annually valued at some $11.5 billion. Billions of dollars are spent annually on the construction and maintenance of asphaltic surfaces on roadways in the US. Nevertheless, existing analysis tools have proven to be inadequate to accurately predict damage accumulation and failure in asphalt pavements. The primary weakness in existing analysis tools is a general lack of understanding of the fundamental mechanisms of fracture and damage in asphaltic composites. Improving a designer's ability to understand and predict the damage-dependent behavior of asphaltic composites will greatly improve structural design of asphaltic roadways.

Accurate prediction and evaluation of damage in asphaltic roadways is challenging, and one of the challenges is related to significant complexities of asphalt mixtures. The asphalt mixtures are classic examples of multiphase, anisotropic, multiscale granular composites consisting of irregularly-shaped and randomly-oriented aggregate particles embedded in the cementitious inelastic matrix phase. In addition to the geometric complexity, inelasticity, and anisotropy, asphalt mixtures have been shown to develop literally thousands of microcracks which eventually coalesce to form macrocracks and then failure due to traffic loading, thus rendering an exact solution untenable. Consequently, most traditional

procedures utilize semi-empirical and/or phenomenological methods and involve repetitive and costly laboratory tests. Phenomenological approaches do not fully account for the fundamental material characteristics, particularly the formation of numerous cracks on multiple length scales that eventually lead to roadway failure. The role played by individual mixture constituents and their effects on the composite constitutive behavior and structures has not been scientifically understood either. Development of a more rigorous, physically based mechanistic model is required in order to predict damage evolution, overall mechanical behavior of mixtures and structures based on better understanding of the mixture constituents and their interactions.

Recently, microstructure-based computational modeling has been actively pursued by many researchers as a means of overcoming the phenomenological approaches. The advantage of the microstructure-based computational modeling approach is that it can account for the effect of mixture heterogeneity by dealing with mixture constituents separately. Several studies [1–6] have proposed the use of finite element method (FEM)-based models to characterize damage performance in asphaltic composites. An explicit numerical technique, called the discrete element method (DEM), has also been used by several researchers [7–9]. These computational approaches have successfully simulated geometric heterogeneity (i.e., random orientation of irregularly shaped aggregates) and have predicted stiffness reduction due to fracture of mixtures subjected to various modes of loading.

Even though various computational techniques based on the mixture microstructure have been shown to be extremely versatile in addressing the microstructural complexities, a composite structure that contains thousands of irregularly-shaped, randomly-oriented inclusions (particles, voids, etc.) along with a number of potential crack sites at different length scales would require a highly refined mesh. The solution for such a problem requires the use of a tremendous amount of computational time and effort, which is rarely feasible with currently available computing power. These limitations have led researchers to seek alternative proper approaches that can account for the hierarchical structure of heterogeneous materials without having to model every microstructural detail, but still considering the most important ones.

One such approach is multiscale modeling as demonstrated in many studies [10–20]. In the multiscale approach, a separate scale analysis is performed at each of the smaller structural scales within the macroscopic body. If statistical homogeneity at any smaller length scale has been satisfied, a homogenization principle is used to produce field equations for the next larger length scale. Damage can also be modeled explicitly at each length scale by incorporating appropriate types of fracture/damage mechanics modeling to the analysis. Therefore, multiscale models more accurately predict structural behavior with much less computational effort by using the homogenized fundamental properties of each of the composite's constituents.

To date, multiscale modeling concepts have rarely been applied to roadway materials and structures. Regarding heterogeneity, inelasticity and damage in multiple length scales in roadway materials and structures, it is obvious that the multiscale modeling-analysis can provide vast advantages in both modeling efficiency and predicting power. The multiscale models can predict larger scale structural behavior with much less computational effort by utilizing the fundamental properties of individual constituents and microstructure characteristics at the smaller scales. Most importantly, the multiscale method can overcome clear obstacles from traditional methods that typically try to model all scales at once.

2 Study objectives and scope

The primary objective of this study is to present a multiscale computational model developed to predict mechanical behavior of viscoelastic asphalt roadways that are subject to fracture damage. The multiscale model is based on continuum thermo-mechanics and is implemented using a finite element formulation. Two length scales (global scale of roadway structure and local scale of mixture) are two-way coupled in the quasi-static model framework by linking a homogenized structure scale to a heterogeneous mixture scale representative volume element (RVE). Along with the theoretical model formulation, model verification and potential applications of the model are provided with example problems. It should be clearly noted that this study is not to validate and calibrate the model with some specific cases but to demonstrate the capabilities of the model developed and verified herein. Therefore, model inputs such as the material properties of mixture components and finite element meshes for the example cases were reasonably determined only for simulation purposes. In addition, the model herein targets only predicting viscoelastic deformation and fracture of mixtures and structures although asphaltic roadways present both viscoelastic fracture damage and plastic deformation.

3 Multiscale initial boundary value problem (IBVP)

The main objective of multiscale models is to determine the overall constitutive behavior of heterogeneous materials simultaneously throughout the analysis based on the behavior of the individual constituents and their interactions at the local scale. Multiscale models become very attractive for problems with evolving microstructure due to formation and growth of microcracks, since the evolution of the microstructure is necessarily both spatially and time dependent, and there are no analytical solutions for this kind of problem, especially for inelastic media. Figure 1 presents an

asphaltic roadway which is considered statistically homogeneous for each layer at the global scale (structure scale) but significantly heterogeneous at the local scale (mixture scale). The size of local mixture scale needs to meet the required dimension of the RVE, since the heterogeneous mixture RVE is homogenized to produce its effective properties that are sequentially updated to the global structure scale constitutive relations. As illustrated in the figure, in the local scale object, various sources of heterogeneity such as particles, voids, and cracks can be considered.

As presented in Fig. 1, the multiscale technique in this study models a global scale object (of its length scale l^G) with its region wherein microcracks (length scale l_c^L) are evolving on the local mixture scale (of its length scale l^L) RVE. The primary variables used in the model are: the displacement vector, the strain tensor, and the Cauchy stress tensor.

3.1 Global scale modeling

In the absence of body forces, inertial effects, and large deformations, a global scale IBVP can be well-posed by an appropriate set of initial-boundary conditions and a set of governing equations: conservation of linear momentum (Eq. (1)), conservation of angular momentum (Eq. (2)), infinitesimal strain-displacement relations (Eq. (3)), and constitutive equations (Eq. (4)).

$$\sigma^G_{ji,j} = 0 \qquad \text{in } V^G \tag{1}$$

$$\sigma^G_{ji} = \sigma^G_{ij} \qquad \text{in } V^G \tag{2}$$

$$\varepsilon^G_{ij} = \frac{1}{2}\left(u^G_{i,j} + u^G_{j,i}\right) \qquad \text{in } V^G \tag{3}$$

$$\sigma^G_{ij}(t) = \bar{\Omega}^{\tau=t}_{\tau=-\infty}\left\{\varepsilon^G_{kl}(\tau)\right\} \quad \text{in } V^G, \tag{4}$$

where σ^G_{ij} = global scale stress tensor, ε^G_{ij} = global scale strain tensor, u^G_i = global scale displacement vector, V^G = volume of global scale body, G indicates global scale, and $\bar{\Omega}^{\tau=t}_{\tau=-\infty}$ is a functional mapping that describes the constitutive behavior at each position in the global object, which may account for damage accumulation and history-dependent effects such as viscoelasticity, and is obtained by locally averaging the response at the local scale RVE to that particular global scale position. Note that Eq. (4) is not known a priori but is determined during the multiscale analysis, which is elaborated in later sections.

3.2 Local scale modeling

Now considering that continuum mechanics still applies at the local scale, assuming that the global length scale is much larger than the local length scale, $l^G \gg l^L$, and that the length scale associated with cracks at the local scale is much smaller than the local length scale, $l^L \gg l^L_c$, that these cracks are homogeneously distributed at the local scale, a well-posed local IBVP is obtained by adjoining uniform initial boundary conditions to the following set of equations:

$$\sigma^L_{ji,j} = 0 \qquad \text{in } V^L \tag{5}$$

$$\sigma^L_{ji} = \sigma^L_{ij} \qquad \text{in } V^L \tag{6}$$

$$\varepsilon^L_{ij} = \frac{1}{2}\left(u^L_{i,j} + u^L_{j,i}\right) \qquad \text{in } V^L \tag{7}$$

$$\sigma^L_{ij}(t) = \Omega^{\tau=t}_{\tau=-\infty}\left\{\varepsilon^L_{kl}(\tau)\right\} \qquad \text{in } V^L \tag{8}$$

$$G^L_i \geq G^L_{iC} \Rightarrow \frac{\partial}{\partial t}\left(\partial V^L_I\right) > 0 \quad \text{in } V^L, \tag{9}$$

where σ^L_{ij} = local scale stress tensor, ε^L_{ij} = local scale strain tensor, u^L_i = local scale displacement vector, V^L = volume of local scale body, L indicates local scale, and $\Omega^{\tau=t}_{\tau=-\infty}$ is a functional that describes the constitutive behavior in the local scale object, G^L_i = fracture energy release rate at a particular position in the local scale, G^L_{iC} = the critical energy release rate of the material, and ∂V^L_I = internal boundary (such as cracks) in the local scale object. It is important to note that Eq. (9) states that cracks can only grow (crack healing is not modeled) and crack growth occurs if the energy release rate overcomes the critical energy release rate of the material.

The functional $\Omega^{\tau=t}_{\tau=-\infty}$ may account for history-dependent effects such as viscoelasticity, and in the current study the functional can represent linear elastic (shown in Eq. (10)) or linear viscoelastic (Eq. (11)) behavior depending on the constituent in the local scale mixture.

$$\sigma^L_{ij} = C^L_{ijkl}\varepsilon^L_{kl} \qquad \text{in } V^L \tag{10}$$

$$\sigma^L_{ij}(t) = \int_{-\infty}^{t} C^L_{ijkl}(t-\tau)\frac{\partial \varepsilon^L_{kl}(\tau)}{\partial \tau}d\tau \quad \text{in } V^L, \tag{11}$$

where C^L_{ijkl} = elastic tensor, $C^L_{ijkl}(t)$ = viscoelastic stress relaxation modulus tensor which is time-dependent, t = time of interest, and τ = integration variable.

The stress relaxation modulus tensor is determined by laboratory relaxation tests, the results of which can be represented by a Prony series as follows:

$$C^L_{ijkl}(t) = C^L_{ijkl,\infty} + \sum_{p=1}^{q} C^L_{ijkl,p}\exp\left(-\frac{C^L_{ijkl,p}}{\eta^L_{ijkl,p}}t\right), \tag{12}$$

where $C^L_{ijkl,\infty}, C^L_{ijkl,p}$ = spring constants, $\eta^L_{ijkl,p}$ = dashpot viscosities, and q = the number of Prony terms in the generalized Maxwell model.

Crack propagation (Eq. (9)) in the local scale can be modeled in many different ways, and one of the well-known approaches is to use a cohesive zone which is illustrated as the fracture process zone in Fig. 1. Cohesive zone models are well-established tools to remove stress singularities ahead of crack tips. Cohesive zone models regard fracture

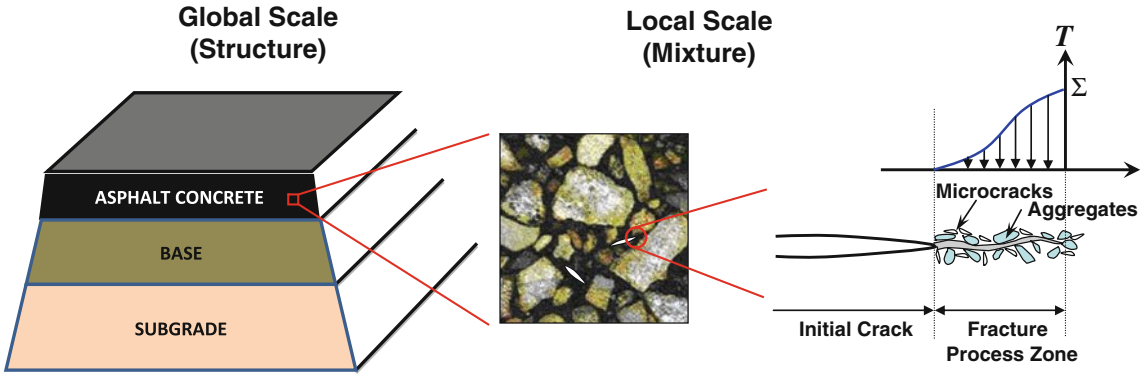

Fig. 1 An asphaltic roadway with two length scales (homogeneous global structure scale and heterogeneous local mixture scale with fracture)

as a gradual phenomenon in which separation takes place across an extended crack tip or cohesive zone (fracture process zone) and where fracture is resisted by cohesive tractions. Since the concept of a cohesive zone was first proposed by Dugdale [21] and Barenblatt [22], many researchers [23–28] have attempted to model the constitutive behavior for cohesive zones.

In an attempt to simulate damage growth due to cracks in viscoelastic media, Yoon and Allen [29] and Allen and Searcy [30,31] formulated a nonlinear viscoelastic cohesive zone model based on micromechanics. This model can reflect nonlinear viscoelastic damage growth and is appropriate for predicting damage evolution, corresponding material softening, and eventual fracture failure of highly inelastic cementitious materials, such as asphalt mixtures. The damage-dependent cohesive zone model which relates cohesive zone traction to cohesive zone opening displacements in viscoelastic media can be written as follows:

$$T_i^L(t) = \frac{1}{\lambda^L(t)} \cdot \frac{u_i^L(t)}{\delta_i^L} \cdot \left[1 - \alpha^L(t)\right] \cdot \left\{ \Sigma_i^L + \int_{t_0}^{t} E^L(t-\tau) \frac{\partial \lambda^L(\tau)}{\partial \tau} d\tau \right\} \text{ on } \partial V_{CZ}^L, \tag{13}$$

where $T_i^L(t)$ = cohesive zone traction, $u_i^L(t)$ = cohesive zone displacements, $\lambda^L(t)$ = Euclidean norm of the cohesive zone displacements, δ_i^L = cohesive zone material length parameter, $\alpha^L(t)$ = internal damage parameter reflecting the area fraction of voids with respect to the cross-sectional area of the idealized cohesive zone, Σ_i^L = required stress level to initiate cohesive zone damage, $E^L(t)$ = relaxation modulus of a single fibril in the cohesive zone, ∂V_{CZ}^L = internal boundary occupied by the cohesive zone, and $i = n$ (normal), or s (shear) for two-dimensional objects.

Similar to the Prony series representation (Eq. (12)) for the bulk viscoelastic element, the relaxation modulus of a single fibril in the cohesive zone can be presented as follows:

$$E^L(t) = E_\infty^L + \sum_{p=1}^{q} E_p^L \exp\left(-\frac{E_p^L}{\eta_p^L} t\right), \tag{14}$$

where E_∞^L, E_p^L = spring constants and η_p^L = dashpot viscosities.

It can be shown that Eq. (13) is mathematically equivalent to Eq. (9), i.e. energy release rate can be computed from the traction-displacement relationship. Conceptually, as the damage parameter $\alpha(t)$ reaches unity, the energy release rate reaches its critical value and the cohesive zone traction vector becomes zero, meaning that a free surface has been created or, equivalently, a crack has propagated.

The damage parameter is determined by performing fracture tests to represent locally averaged cross-sectional area of damaged material in a cohesive zone. Alternatively, a phenomenological form of the damage evolution can also be employed to represent rate-dependent fracture. In the current study, the following simple phenomenological form [31] has been selected, since it is sufficient to demonstrate the formation and applicability of the multiscale model.

$$\dot{\alpha} = A\left[\lambda(t)\right]^m, \qquad \text{when } \dot{\lambda} > 0 \text{ and } \alpha < 1 \tag{15}$$

$$\dot{\alpha} = 0, \qquad \text{when } \dot{\lambda} \le 0 \text{ or } \alpha = 1, \tag{16}$$

where A and m are microscale material constants which govern damage evolution behavior.

Since cohesive zone elements may introduce additional compliance to the finite element mesh prior to crack initiation and increase the maximum bandwidth of the stiffness matrix, the computational model used herein provides an algorithm to adaptively insert cohesive zone elements into the finite element mesh at the moment at which the criterion for cohesive zone initiation is satisfied such as:

$$T_i^L(t) \ge \Sigma_i^L \tag{17}$$

For a given solution step, the stress tensor is computed at every node in the mesh and then the traction vector is computed for every elemental edge sharing that node using Cauchy's formula. Then, the traction vector for every edge in the

mesh is checked against the crack initiation criterion (Eq. (17)). Finally, if the crack initiation criterion is satisfied for certain edge node, this node is doubled and a cohesive zone element is then created for the new surface. One more thing to be noted is that the Lagrange multipliers technique is used in the model to apply displacement constraints in the cohesive zone elements so that nodal interpenetration is precluded. Further details on the algorithm for adaptive insertion of cohesive zones can be found elsewhere [32,33].

3.3 Homogenization for linking two scales

Homogenization principles can now be used to establish the relationships connecting both length scales. Accumulated damage and structural degradation resulting from the local scale analysis influence constitutive behavior at the global scale. The results from the local scale analysis are homogenized and linked to the global scale problem. The concept of homogenization [34,35] is applicable when the heterogeneous medium satisfies statistical homogeneity. Homogenization is central to the idea of multiscaling and is typically through the averaging process of local fields within the heterogeneous medium as follows:

$$f^G(x_i^G, t) = \bar{f}^L \equiv \frac{1}{V^L}\int\limits_{V^L} f^L(x_i^L, t)dV, \tag{18}$$

where $\bar{f}$ = volume average of a generic function f, f^G = the function at the global scale, f^L = the function at the local scale, and x_i^L = the spatial coordinate at the local scale.

Using the divergence theorem, one can transform the volume integral above to a surface integral equation. Therefore, if the boundary conditions at the local scale are homogeneous, the homogenized stresses at the global scale in terms of the local stresses can be written as follows:

$$\sigma_{ij}^G = \bar{\sigma}_{ij}^L \equiv \frac{1}{V^L}\int\limits_{\partial V_E^L} \sigma_{ki}^L n_k^L x_j^L dS, \tag{19}$$

where ∂V_E^L = external boundary of the local scale RVE, and n_k^L = the unit outer normal vector to the volume of local scale RVE.

Likewise, the homogenized strains at the global scale in terms of the local strains can be expressed as follows:

$$\varepsilon_{ij}^G = \bar{\varepsilon}_{ij}^L = E_{ij}^G + e_{ij}^G \tag{20}$$

$$E_{ij}^G = \bar{E}_{ij}^L \equiv \frac{1}{V^L}\int\limits_{\partial V_E^L} \frac{1}{2}\left(u_i^L n_j^L + u_j^L n_i^L\right) dS \tag{21}$$

$$e_{ij}^G = \bar{e}_{ij}^L \equiv \frac{1}{V^L}\int\limits_{\partial V_I^L} \frac{1}{2}\left(u_i^L n_j^L + u_j^L n_i^L\right) dS, \tag{22}$$

where $\bar{E}_{ij}^L$ = external boundary average strain tensor, $\bar{e}_{ij}^L$ = internal boundary average strain tensor which represents an averaged measure of damage due to cracks in the local scale RVE.

The use of Eqs. (19)–(22) is termed a mean field theory of homogenization because the behavior of the global object is determined only in terms of the mean stress and strain tensors evaluated at the boundary of the local RVE. In the case of quasi-static problems such as the one discussed in this paper, the computation of the homogenized constitutive tensor is obtained in order to correctly calculate the tangent stiffness matrix $\bar{\Omega}_{\tau=-\infty}^{\tau=t}$ which is involved in Eq. (4).

It is important to note that the assumption that the strain tensor is spatially uniform along the external boundary of the RVE breaks down in regions of high gradients, such as in the vicinity of cracks or where the size of the RVE is comparable to the global length scale. Higher order homogenization theorem can however be formulated by including gradients of the deformation and moments of the stress tensor in the model [36].

4 Incremental formulation for time dependence

When the IBVP is time and/or history dependent such as the problem herein, incrementalization is necessary to allow integration of the governing equations, at least in an approximate manner. Therefore, the multiscale model in this study uses an incremental scheme for viscoelastic solids containing cracks. Theoretical details demonstrating individual steps related to the incremental formulation can be found in other studies [32,37,38]; therefore, final equations in a summarized form are presented in this paper for a complete discussion.

The stress tensor and the cohesive zone traction vector at local scale RVE can be written in incremental form such as:

$$\sigma_{ij}^L(t+\Delta t) = \sigma_{ij}^L(t) + \Delta\sigma_{ij}^L \tag{23}$$

$$T_i^L(t+\Delta t) = T_i^L(t) + \Delta T_i^L \tag{24}$$

Assuming that the strain rate is constant for each time step and that the linear viscoelastic relaxation modulus is represented by a Prony series (as shown in Eq. (12)), the following incremental constitutive equation can be expressed for the local scale RVE [37].

$$\Delta\sigma_{ij}^L = C_{ijkl}^L \Delta\varepsilon_{kl}^L + \Delta\sigma_{ij}^{RL}, \tag{25}$$

$$\text{where } C_{ijkl}^L = C_{ijkl,\infty}^L + \frac{1}{\Delta t}\sum_{p=1}^{q}\eta_{ijkl,p}^L\left\{1-\exp\left(-\frac{C_{ijkl,p}^L}{\eta_{ijkl,p}^L}\Delta t\right)\right\} \tag{26}$$

$$\Delta\sigma_{ij}^{RL} = -\sum_{k=1}^{3}\sum_{l=1}^{3} A_{ijkl}^L \tag{27}$$

$$A^L_{ijkl} = \sum_{p=1}^{q} \left\{ 1 - \exp\left(-\frac{C^L_{ijkl,p}}{\eta^L_{ijkl,p}} \Delta t \right) \right\} \cdot S^L_{ijkl,p}(t) \quad (28)$$

$$S^L_{ijkl}(t) = \exp\left(-\frac{C^L_{ijkl,p}}{\eta^L_{ijkl,p}} \Delta t \right) \cdot S^L_{ijkl,p}(t - \Delta t) + \eta^L_{ijkl,p} \cdot \frac{\Delta \varepsilon^L_{kl}}{\Delta t} \cdot \left\{ 1 - \exp\left(-\frac{C^L_{ijkl,p}}{\eta^L_{ijkl,p}} \Delta t \right) \right\} \quad (29)$$

In a similar way, the time increment of the viscoelastic cohesive zone traction in the local scale RVE can also be derived, and the resulting recursive traction difference ΔT^L_i between time t and $t + \Delta t$ is expressed as follows [38]:

$$\Delta T^L_i = k^L_{ij} \Delta u^L_j + \Delta T^{RL}_i, \quad (30)$$

$$\text{where } k^L_{ij} = \frac{[1 - \alpha^L(t + \Delta t)]}{\delta^L_i} \cdot \left[E^L_\infty + \frac{1}{\Delta t} \sum_{p=1}^{q} \eta^L_p \left\{ 1 - \exp\left(-\frac{E^L_p}{\eta^L_p} \Delta t \right) \right\} \right] \quad (31)$$

$$\Delta T^{RL}_i = \frac{[1 - \alpha^L(t)]}{\delta^L_i} \left[-\sum_{p=1}^{q} \left\{ 1 - \exp\left(-\frac{E^L_p}{\eta^L_p} \Delta t \right) \right\} \cdot s^L_{ij}(t) \right] - \frac{\Delta \alpha^L}{\delta^L_i} \left[E^L_\infty \cdot u^L_i(t) + \sum_{p=1}^{q} s^L_{ij}(t) - \sum_{p=1}^{q} \left\{ 1 - \exp\left(-\frac{E^L_p}{\eta^L_p} \Delta t \right) \right\} \cdot s^L_{ij}(t) \right] - \Delta \alpha^L \cdot \Sigma^L_i \quad (32)$$

$$s^L_{ij}(t) = \exp\left(-\frac{E^L_p}{\eta^L_p} \Delta t \right) \cdot s^L_{ij}(t - \Delta t) + \frac{\Delta u^L_i}{\Delta t} \cdot \eta^L_p \cdot \left[1 - \exp\left(-\frac{E^L_p}{\eta^L_p} \Delta t \right) \right] \quad (33)$$

Now assuming that the homogenized constitutive behavior of the global scale object can be approximated by an incremental form similar to Eqs. (23) and (25):

$$\sigma^G_{ij}(t + \Delta t) = \sigma^G_{ij}(t) + \Delta \sigma^G_{ij} \quad (34)$$

$$\Delta \sigma^G_{ij} = C^G_{ijkl} \Delta \varepsilon^G_{kl} + \Delta \sigma^{RG}_{ij} \quad (35)$$

C^G_{ijkl} is the homogenized algorithmically consistent tangent tensor, which is a function of time through its dependence on the amount of damage accumulated at the local RVE, and $\Delta \sigma^{RG}_{ij}$ is the so-called homogenized history-dependent residual stress term, which represents the history- and rate-dependence in the material (both bulk and cohesive zones) behavior. Using the concept of localization tensors [39] with an assumption postulating that the local displacement field can be related to the global strain tensor [40], the homogenized instantaneous constitutive tensor and the homogenized history-dependent residual stress term can be derived, respectively as follows:

$$C^G_{ijkl} = \frac{1}{V^L} \int_{V^L} \left[C^L_{ijkl} + C^L_{ijmn} \left\{ \frac{1}{2} \left(\Lambda^L_{mkl,n} + \Lambda^L_{nkl,m} \right) \right\} \right] dV \quad (36)$$

$$\Delta \sigma^{RG}_{ij} = \frac{1}{V^L} \int_{V^L} \left(C^L_{ijkl} \Delta \varepsilon^{RL}_{kl} + \Delta \sigma^{RL}_{ij} \right) dV, \quad (37)$$

$$\text{where } \Delta \varepsilon^{RL}_{ij} = \frac{1}{2} \left(\Delta u^{RL}_{i,j} + \Delta u^{RL}_{j,i} \right) \quad (38)$$

Λ^L_{ijk} is called the localization tensor that is necessary to address the local displacement field due to the existence of local asperities and internal boundaries including cracks and cohesive zones. As shown in Eq. (36), the global scale tangent tensor is controlled by heterogeneity, internal boundaries, and cracks at the local scale RVE through the localization tensor, and is also affected by viscoelasticity through local scale viscoelastic property $C^L_{ijkl}(t)$. Therefore, the amount of damage accumulated at the local scale RVE produces a nonlinear behavior at the global scale. The homogenized residual stress term is estimated by the local scale property and the local scale stress and strain fields, which are identified by Eq. (27) and Eq. (38), respectively. Therefore, it is obvious that the homogenized quantities at the global scale object are obtained from the local scale RVE with given expressions of the localization tensor in Eq. (36) and the local scale history-dependent displacement fields in Eq. (38). Souza and Allen [32] presented a concise theoretical framework of this two-way multiscale model and the corresponding finite element formulation. The following matrix forms were finally developed:

$$\left[\Lambda^L \right] = -\left[K^L \right]^{-1} \left[G^L \right] \quad (39)$$

$$\left\{ \Delta u^{RL} \right\} = \left[K^L \right]^{-1} \left\{ F^{RL} \right\}, \quad (40)$$

$$\text{where } \left[K^L \right] = \int_{V^L} \left[B^L \right]^T \left[C^L \right] \left[B^L \right] dV + \int_{\partial V^L_{CZ}} \left[N^L \right]^T \left[k^L \right] \left[N^L \right] dS \quad (41)$$

$$\left[G^L \right] = \int_{V^L} \left[B^L \right]^T \left[C^L \right] dV \quad (42)$$

$$\left\{ F^{RL} \right\} = -\int_{V^L} \left[B^L \right]^T \left\{ \Delta \sigma^{RL} \right\} dV - \int_{\partial V^L_{CZ}} \left[N^L \right]^T \left\{ \Delta T^{RL} \right\} dS \quad (43)$$

$[N^L]$ = shape functions, and $[B^L]$ = spatial derivatives of shape functions.

The multiscale model herein is considered a two-way coupled model because the applied displacements on the boundary of the local scale are computed from the global scale strain tensor (global-to-local coupling), and the homogenized quantities are obtained from the solution of the local scale IBVP (local-to-global coupling). Figure 2 presents the two-way coupled multiscale modeling algorithm in a flowchart form. Basically, the model is operated with seven major steps: (i) read inputs for global and local scales; (ii) obtain initial homogenized tangent tensor for global problem; (iii) solve the global problem at a given time step; (iv) apply global scale solution to local scale boundary value problem; (v) solve the local scale problem at the time step; (vi) homogenize local scale results; and (vii) update homogenized local scale results to the global scale object at each integration point for the next time step. It should be mentioned that, even though not shown in Fig. 2, for each global scale nonlinear time step, an iterative Newton-Raphson loop is performed to guarantee convergence. The two-way coupled multiscale model with all features described has been implemented into a commercial finite element software package MultiMech^{TM} provided by MultiMech Research and Development, LLC. The following model simulations were conducted by using the MultiMech^{TM}.

5 Model verification

In order to verify the multiscale computational model developed, a heterogeneous tapered bar as presented in Fig. 3 is introduced. The tapered bar is a composite consisting of viscoelastic matrix and elastic particles. Due to the axis of symmetry, only half of the bar is modeled, and monotonically increasing displacements are applied at the right end of the bar, as shown in the figure. For the multiscale analysis, a local scale microstructure describing the important geometric heterogeneities is needed. In the present example, a unit cell is selected which possesses the same volume fraction and equal level of mesh refinement obtained from the single scale reference mesh. Model verification was performed in two separate forms: without and with microstructure evolution such as cracks and/or cohesive zones with time.

For the case without the microstructure evolution, the multiscale computational solutions are compared to solutions that can be analytically obtained as well as simulation results from the single scale reference case where all heterogeneities in the tapered bar are explicitly modeled in the global scale mesh. The good agreement between model predictions and the analytic solutions verify model accuracy of the multiscale technique, and the comparison in the simulation time between multiscale model and the single scale model shows the modeling efficiency of the multiscale approach compared to the single scale technique.

For the case with microstructure evolution due to damage over time, any deviation of computational simulations from the undamaged analytic solutions will identify the amount of damage predicted by the computational modeling approaches. Since no analytic solution is available for the problems including material viscoelasticity, heterogeneity, and rate-dependent fracture, the predicting accuracy of the multiscale model will only be estimated by comparing multiscale model simulations with simulation results from the single scale model. Furthermore, simulation time between two approaches can be compared to estimate the modeling efficiency.

The global and local scale objects are discretized and the finite element meshes are constructed as shown in Fig. 3. The finite element mesh (15,437 triangular elements) shown in Fig. 3b of the global scale object with particles (Fig. 3a) was finally developed by repeating a mesh refinement process until the single scale finite element numerical solution converges and closes to analytic solutions which are provided later. In order to verify the multiscale modeling technique, a homogeneous global scale mesh with only eight triangular elements as presented in Fig. 3d is simulated by linking with the local scale unit cell (shown in Fig. 3c) which contains 72 triangular elements. Simulation results from the multiscale model can then be compared to the single scale (Fig. 3b) reference simulation and the analytic solution. Table 1 presents material properties of the local scale constituents (i.e., elastic particles, viscoelastic matrix, and cohesive zone properties for the case with microcracks). Only local scale properties are necessary to complete the local-global multiscale simulation. The properties used are arbitrarily assumed for simulation purposes only.

For the case without microstructure evolution, the analytic solution is given as follows:

$$\varepsilon_{xx}(x,t) = \frac{0.1t}{0.693} \cdot \left(\frac{1}{20-x}\right) \tag{44}$$

$$\sigma_{xx}(x,t) = \frac{0.1}{0.693} \cdot \left(\frac{1}{20-x}\right) \cdot \hat{E}(t), \tag{45}$$

$$\text{where } \hat{E}(t) = \hat{E}_\infty t - \sum_{p=1}^{q} \hat{\eta}_p \left\{1 - \exp\left(-\frac{\hat{E}_p}{\hat{\eta}_p} t\right)\right\} \tag{46}$$

$\hat{E}_\infty, \hat{E}_p, \hat{\eta}_p$ = Prony series terms evaluated for the composite tapered bar.

Figure 4 plots the average stresses (σ_{xx}) of the tapered bar as loading time increases. Based on the results presented in Fig. 4, the following remarks can be drawn: (i) the single scale simulation results are almost identical to the analytic solution, which infers that the single scale mesh is sufficiently fine, and (ii) the accuracy of the multiscale model increases as the global scale mesh is refined, but in this case

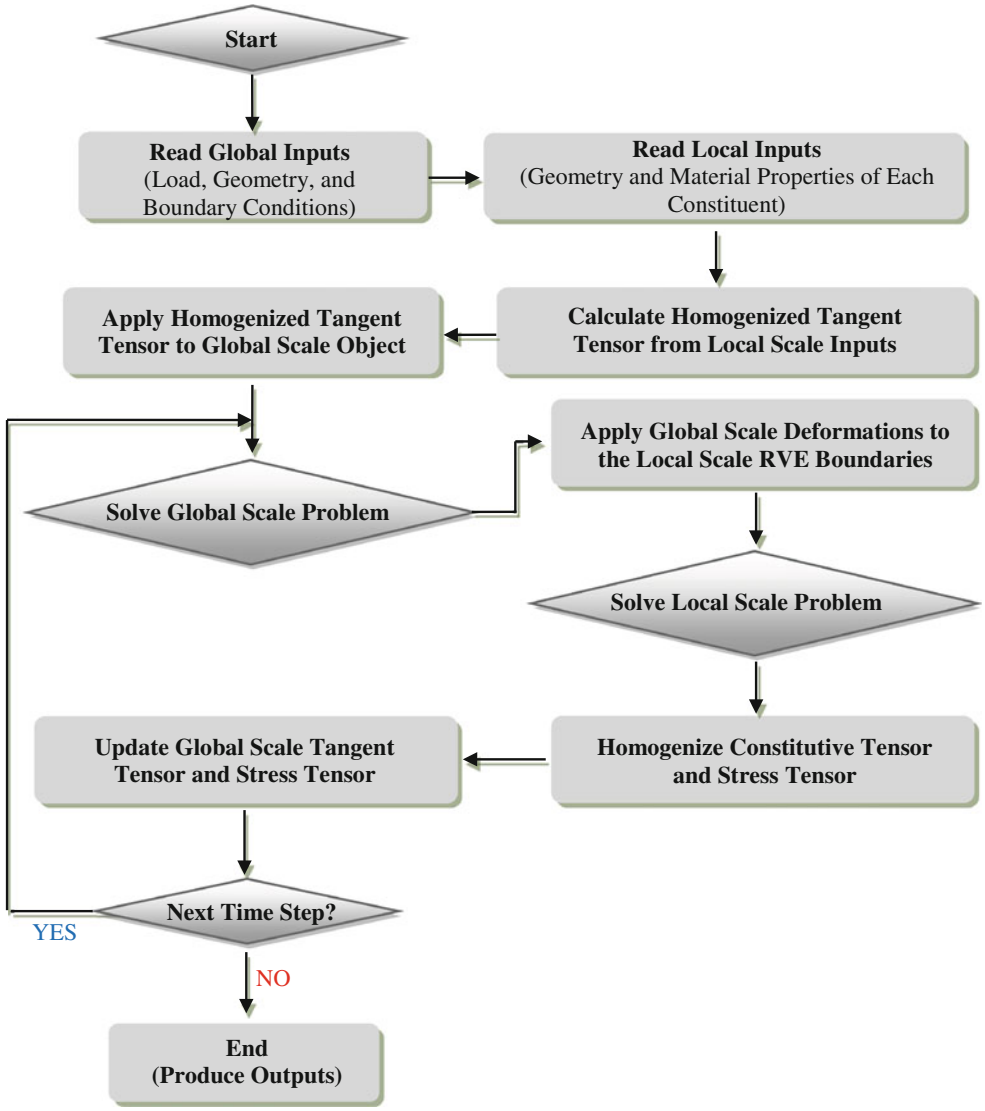

Fig. 2 A *flowchart* describing the two-way coupled multiscale modeling algorithm

only 8 constant strain triangle elements for the global scale and 72 constant strain triangles for each local scale mesh suffice, as opposed to 15,437 elements needed by the single scale reference simulation. This result points out the efficiency of the multiscale approach. The amount of time required to complete the single scale reference simulation was about 18.5 min, while the same level of accuracy could be obtained from the multiscale model in 37 s using an ordinary desktop computer with only one processor (2.50 GHz CPU, 4GB RAM memory, and Linux OS). Furthermore, the multiscale model can also run in parallel computing environments, which highlights the benefit of multiscale modeling approach. The parallel computing vastly reduce simulation time, since individual local scale IBVPs can be solved in parallel by multiple processors.

For the cases where the microstructure does not evolve with time and/or loading history, the two-way couple multiscaling is not necessarily required since the same degree of accuracy can be obtained by using the simpler classical homogenization theory. The two-way coupled multiscale models are however very attractive for problems where the microstructure evolves with time, such as when microcracks initiate and propagate. It is therefore now necessary to verify the code for cases where damage evolves in the microstructure.

The effectiveness of the model for damage-induced problems was verified by simulating the same tapered bar problem by comparing single scale simulation results with multiscale results. However, different from the previous case, cohesive zone elements are now adaptively inserted into the mesh once the cohesive zone initiation criterion (presented in Eq. (17)) is met. Even though fracture problems typically require higher level of mesh refinement, the same mesh used for the non-damage case was adopted here so that one can

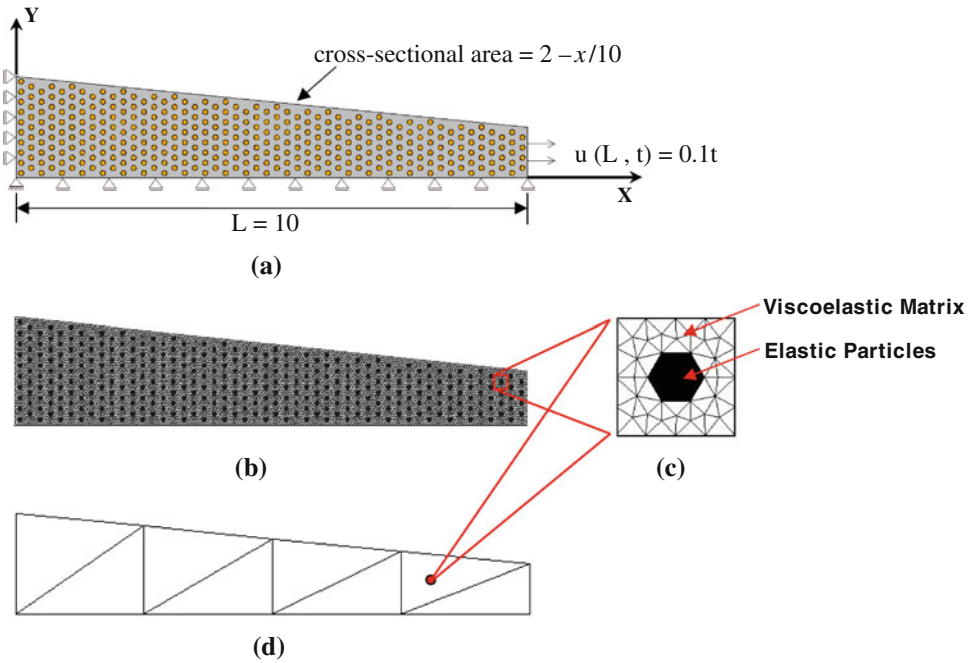

Fig. 3 Elastic-viscoelastic tapered bar problem to check model accuracy and efficiency. **a** Tapered bar with particles. **b** Single scale mesh. **c** Local mesh for the multiscale. **d** Global mesh for the multiscale

Table 1 Local scale material properties used for the tapered bar problem

Elastic particles		Viscoelastic matrix		
E (GPa)	55.2		ν	0.35
ν	0.15	p	E_p (MPa)	η_p (MPa s)
		∞	7.02	N/A
		1	245.65	0.00737
Cohesive zone in the matrix[a]		2	422.26	0.1267
δ_n (m)	0.05	3	399.32	1.198
δ_s (m)	0.05	4	251.83	7.555
Σ_n (MPa)	1.50	5	69.10	20.729
Σ_s (MPa)	1.50	6	22.59	67.757
A	10.0	7	7.82	234.497
m	0.50	8	3.46	1037.880

[a] Same fracture properties were used to normal and shear directions for simplicity

compare computational times for both cases. Figure 5 plots the average stress (σ_{xx}) of the tapered bar as loading time increases.

Due to the formation of cohesive zones followed by cracks, it can be noticed in Fig. 5, that the average stress deviates from the non-damage (linear viscoelastic) curve (presented by the analytical solution). The multiscale solution was considered satisfactory when compared to the single scale simulation results, which verifies the accuracy of the multiscale model for damage-induced problems. In terms of computational time required to run this problem, the multiscale solution was obtained approximately 250 times faster than the single scale case. 26,700 s were necessary to complete the single scale case, whereas only 105 s were used to run the multiscale problem. Clearly, this example demonstrates the higher computational efficiency of the multiscale technique when the object is highly heterogeneous and contains damage. This benefit will further be noticeable when one models geomaterials and infrastructure that typically presents a significant level of geometric complexity and material inelasticity.

Figure 6 presents the deformed mesh and elemental stresses of the tapered bar for the single scale case (Fig. 6a) and the multiscale case (Fig. 6b), respectively. As shown, the tapered bar experiences higher stress as the cross-sectional area of the bar decreases, and particles are under higher stresses than the matrix phase as shown in the single scale simulation (Fig. 6a). The homogenized stresses obtained from the multiscaling seem to be equivalent to the stress state of the single scale case where two phases (i.e., particle and matrix) clearly present different level of stresses. In addition, cohesive zones (represented by solid lines) inserted into individual RVEs clearly demonstrate the spatially-dependent damage characteristics of the tapered bar problem.

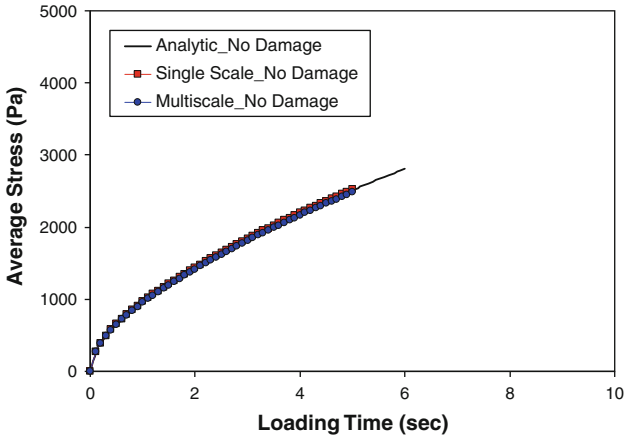

Fig. 4 Model simulation results and comparisons with analytic solution without damage

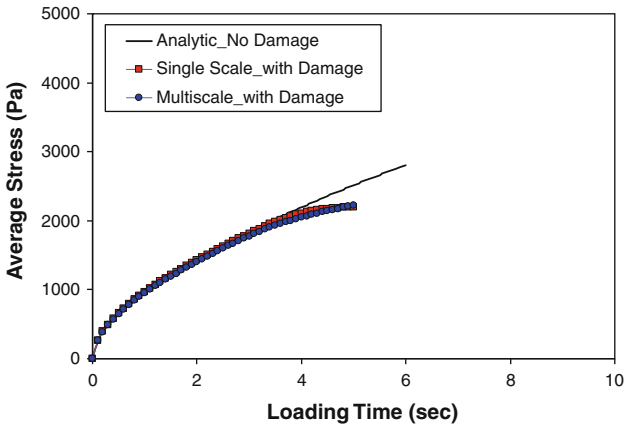

Fig. 5 Model simulation results and comparisons with analytic solution with damage

6 Model application

In order to demonstrate the applicability of the multiscale model to composite structures where material inelasticity and fracture damage are incorporated, an asphaltic roadway structure subject to a cyclic loading was modeled. The roadway structure to be modeled herein was arbitrarily constructed with typical three layers; 0.1-m thick asphaltic surface, 0.1-m thick aggregate base layer, and 1.3-m thick soil subgrade; as shown in Fig. 7. The asphaltic surface layer is homogeneous in the global point of view but is modeled through the two-way couple multiscale by linking all 253 global scale elements to respective local scale heterogeneous RVE mixture. Thus, anisotropic and inelastic behavior of the surface layer due to mixture viscoelasticity, spatial distribution of the aggregates, and directional evolution of cohesive zones and microcracks is automatically addressed by the scale linking. The second and third layers were modeled as isotropic linear elastic without linking to their local scale RVEs. Only the surface layer is modeled by the multiscale approach in this example for modeling simplicity, although all three layers can be modeled through the multiscale method with their corresponding RVEs.

For the local scale, a 0.05-m by 0.05-m asphalt concrete mixture has been arbitrarily chosen as a RVE based on recent findings by Kim et al. [41,42]. To determine appropriate RVE dimensions of asphalt concrete mixtures, Kim et al. [41,42] attempted multiple approaches such as geometrical analysis of mixture heterogeneity using actual images of mixture microstructure, experimental evaluation through mechanical tests incorporated with digital image correlation technique, and numerical simulation of mixture microstructures. Each analysis presented similar results indicating that typical dense-graded asphalt mixtures can be characterized for their material properties with an approximate RVE size of 0.05–0.06 m.

As presented in Fig. 7, the local scale RVE consists of elastic coarse aggregates and viscoelastic asphalt matrix which mixes asphalt binder with fine aggregates and additives. The coarse aggregate particles in the local scale are modeled as linear elastic, whereas the asphalt matrix phase is viscoelastic with fracture. Adaptive insertion of viscoelastic cohesive zones is allowed in the matrix material to simulate rate-dependent damage in the form of discrete cracks at the local scale. As mentioned earlier, other roadway distresses such as plastic deformation or moisture damage were not considered in this example. This model application targets only predicting viscoelastic deformation and fracture of mixtures and structures.

Since the purpose of this example is not to accurately model some specific structures for validation but to demonstrate the capabilities of the model to account for material heterogeneity, inelasticity, and fracture with significantly reduced computational efforts through the two-way couple scale linking, the roadway structure was modeled with two-dimensional axisymmetric approximation with reasonably determined finite element meshes. Axisymmetric modeling is limited in accounting for realistic tire loading and axle configurations, but it can properly provide important physical insights with considerable savings in computational efforts with comparable model accuracy compared to three-dimensional modeling. Therefore, it has been used by many researchers for the modeling of roadway structures. In addition, as shown in Table 2, material properties of the asphalt concrete mixture constituents and underneath layers were assumed with reasonable typical values. The cohesive zone properties of asphalt matrix phase in the local mixture RVE were also arbitrarily assumed for simulation purposes only, even though they can be directly measured by performing laboratory fracture tests [43–45].

Figure 7 also shows the loading sequence applied to the roadway. Although the loading condition is not uniform in

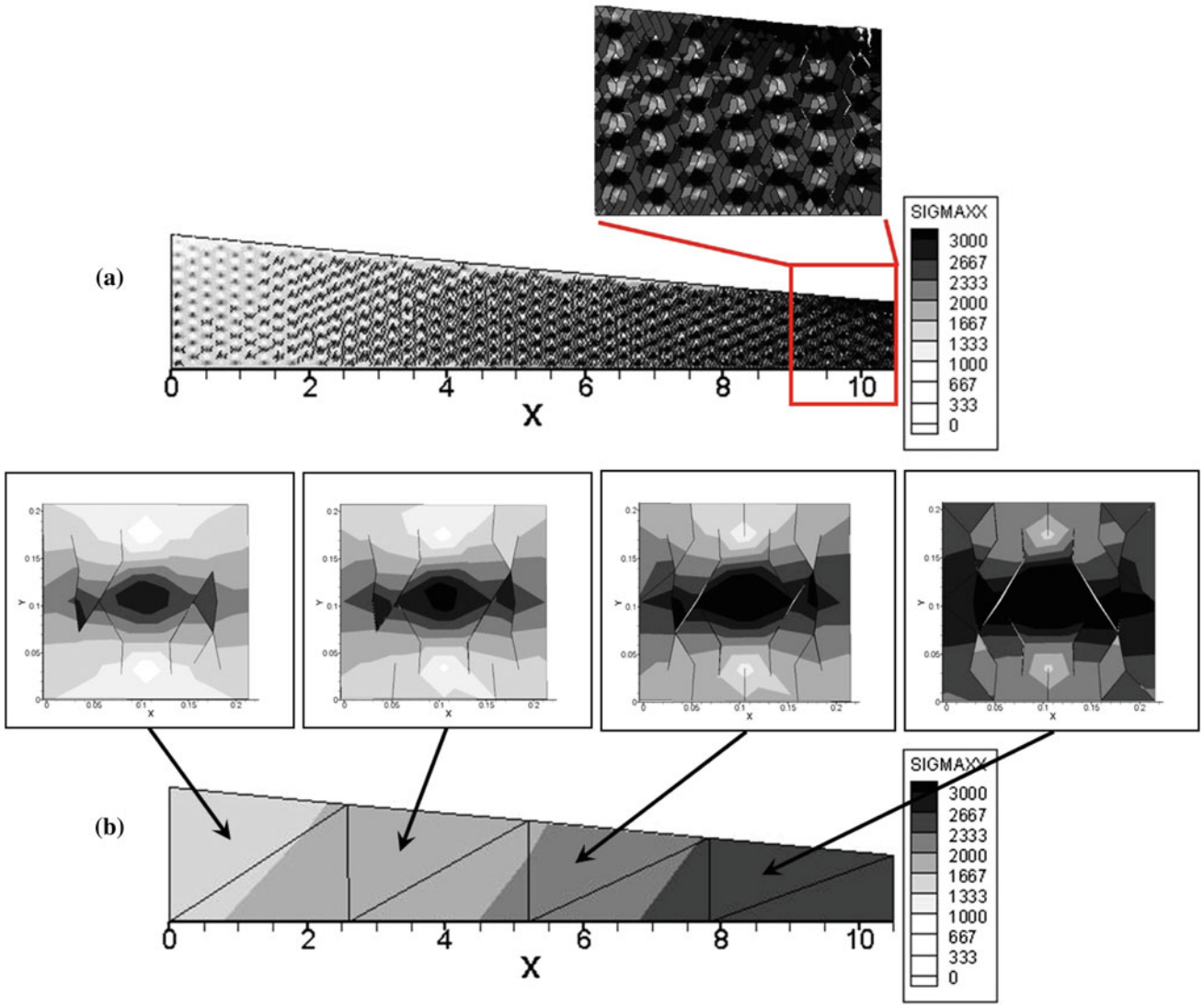

Fig. 6 Deformed meshes and elemental stresses of the tapered bar

reality, for the current study, a uniformly-distributed circular load (0.15-m radius) with its magnitude of 18.75 kN was applied for simulating a passage of a typical dual-tire truck axle (75 kN). To represent multiple passages, the loading sequence was applied repeatedly with a 0.1-s loading pulse followed by a 0.9-s rest period.

Simulation results were represented in a form of snapshots for both global structure and local RVE mixtures. Snapshots taken at peak of two different loading cycles (7th and 12th) are given in Fig. 8. The global structure results are presented in a contour plot of stress components σ_{xx} (horizontal), σ_{yy} (vertical), and σ_{xy} (shear). Four local RVEs (A, B, C, and D) were strategically selected at four different locations in the global scale and their deformation characteristics with cohesive zone development at the 12th loading cycle are presented in the figure. Local scale RVEs A and B represent the mixture behavior on top of the asphalt surface layer at two different important locations: in the middle of tire loading zone (RVE A) and at the edge of tire loading (RVE B). Mixture RVE C was selected to investigate damage-dependent mixture behavior at the bottom of the asphalt layer in the center of tire loading, which has traditionally been known as a critical location developing bottom-up fatigue cracks, whereas RVEs A and B are more closely related to top-down cracking. Mixture RVE D which is far from the loading can be compared to other RVEs that are more directly influenced by the tire loading, so that spatially-dependent damage characteristics due to the loading can be visualized.

As can be clearly seen, the roadway presents higher stresses with the increasing number of loading cycles, which indicates the fatigue damage process. In this particular example, with the given loading conditions, material properties, and

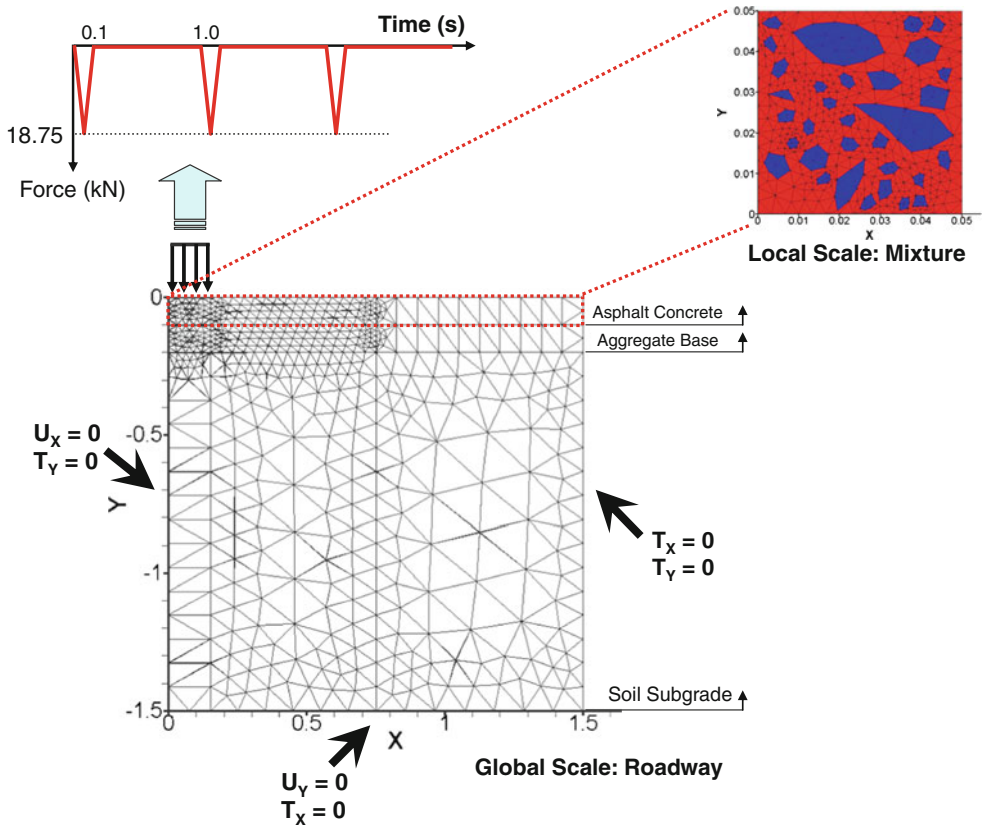

Fig. 7 Three-layer roadway structure to demonstrate applicability of the multiscale model

Table 2 Material properties used for the roadway problem

Bulk materials				
Elastic particles in local RVE		Asphalt matrix in local RVE		
E (GPa)	60.9		ν	0.35
ν	0.15	p	E_p (MPa)	η_p (MPa s)
		∞	12.15	–
Elastic properties of aggregate base		1	2497.50	0.2497
E (GPa)	0.20	2	1363.50	1.364
ν	0.40	3	1026.50	10.26
		4	302.40	30.24
Elastic properties of soil subgrade		5	120.69	120.69
E (GPa)	0.06	6	36.45	364.50
ν	0.45	7	9.02	901.80
		8	1.47	1474.20
Cohesive zone properties of asphalt matrix in local RVE[a]				
δ_n (m)	0.001			
δ_s (m)	0.001			
Σ_n (MPa)	1.0			
Σ_s (MPa)	1.0			
A	1.0			
m	0.5			

[a] Same fracture properties were used to normal and shear directions for simplicity

geometry, the roadway structure is subject to compressive stress through the entire surface layer, while significant tensile stress is observed around the bottom of base layer, which results in potential sites for crack propagation in opening mode. At the top of surface layer, although the roadway is under significant compression due to tire loading, the com-

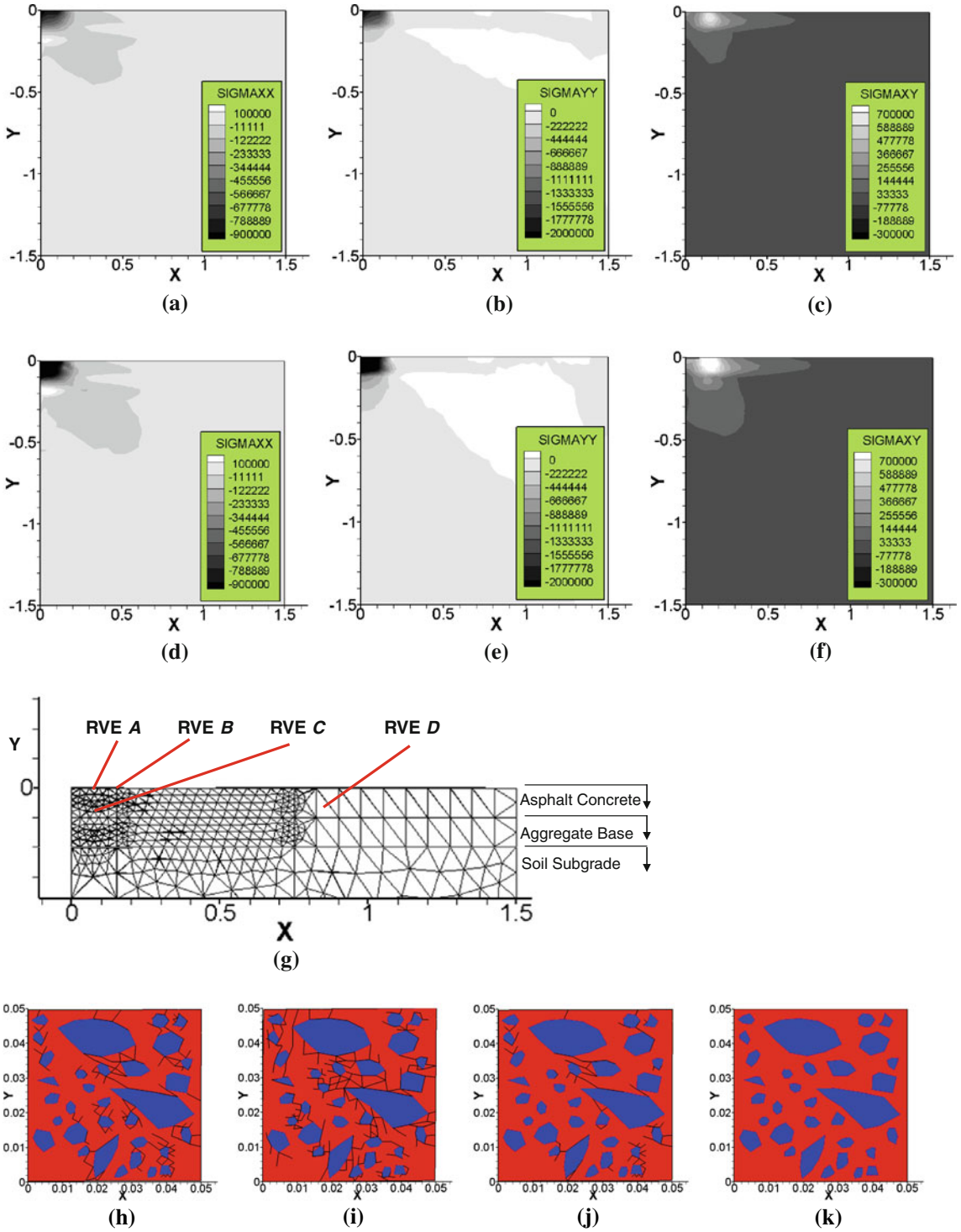

Fig. 8 Multiscale simulation results of the roadway problem. **a** σ_{xx} at 7th cycle. **b** σ_{yy} at 7th cycle. **c** σ_{xy} at 7th cycle. **d** σ_{xx} at 12th cycle. **e** σ_{yy} at 12th cycle. **f** σ_{xy} at 12th cycle. **g** RVE locations in the global scale. **h** RVE *A* at 12th cycle. **i** RVE *B* at 12th cycle. **j** RVE *C* at 12th cycle. **k** RVE *D* at 12th cycle

pressive stress develops damage in shear as presented in the deformation contour of the RVE *A* where a number of cohesive zone elements (represented by solid lines) are embedded. Damage associated with shear is even more visible at the edge of tire loading. Structure contour of σ_{xy} and the cohesive zones developed in the RVE *B* in the figure demon-

strate potential crack propagation in shearing mode, which is in agreement with other studies [46,47] that investigated the mechanisms of top-down cracking. In the case of the RVE that is far away from the loading zone, no significant damage is involved in the microstructure, as seen from the RVE D. Similar analyses can be conducted at any target conditions: loading conditions, individual properties of materials, and roadway geometries.

The multiscale model accounts for the effects of microstructural details by using a local scale RVE with significantly reduced amount of computational effort and laboratory tests due to the use of only local scale constituent properties, as opposed to mixture properties. Therefore, in evaluating the effect of mixture volumetric and/or microstructural characteristics on the overall damage-induced performance of mixtures and structures, no laboratory experiments would be further required since the mixture characteristics are computed through the model.

Although, this study did not target to present modeling sensitivity related to the local scale constituent properties, it is not premature to expect that the multiscale model can allow roadway engineers to better understand the mechanical effects of material-specific design variables on the overall damage-related responses and performance characteristics of structures. Consequently, the better understanding of small-scale design variables can help engineers select mixture constituents in a more appropriate way and advance the current volumetric mix-design concepts, materials models, and performance prediction models.

7 Summary and conclusions

This paper described the theoretical framework of a computational multiscale model with its verification and potential applications to predict mechanical behavior of viscoelastic asphalt roadways that are subject to nonlinear, inelastic fracture damage. Two physical length scales were two-way coupled in the quasi-static finite element framework by linking a homogenized global scale to a heterogeneous local scale RVE. Based on the unique multiscale algorithm, it was possible to take into account the effect of mixture heterogeneity, inelasticity, and anisotropic damage accumulation in the small scale on the overall performance of larger scale structures. The nonlinear viscoelastic cohesive zone model was also incorporated in the model to address rate-dependent fracture damage in the asphaltic mixtures and roadway structures.

The model demonstrated clear potential and significant benefits compared to traditional approaches in that only local scale properties and local scale microstructure characteristics are necessary to model damage-induced behavior in larger scale objects. This results in significant savings in time and costs. Furthermore, compared to single scale computational modeling of heterogeneous objects, the multiscale model demonstrated much higher computational efficiency by reducing simulation time based on the homogenization process to link scales and the parallel computing capabilities which highlight the benefit of multiscale modeling approach.

It is expected that a successfully developed multiscale computational model, such as the one presented herein, can be an efficient analysis-design-prediction tool for various types of mixtures and structures including asphalt mixtures and roadways targeted in this study. Although many challenges still exist, and further improvements are necessary remain for the future studies, this paper demonstrates the potential power and efficacy of this modeling approach.

Acknowledgments The authors are grateful for the financial support received from the National Science Foundation (Grant No. CMMI-0644618). We also appreciate MultiMech Research and Development, LLC for providing courtesy license of multiscale software package MultiMech^{TM} during performance of this work.

References

1. Masad E, Niranjanan S, Bahia H, Kose S (2001) Modeling and experimental measurements of localized strain distribution in asphalt mixes. J Transp Eng 127(6):477–485
2. Papagiannakis AT, Abbas A, Masad E (2002) Micromechanical analysis of viscoelastic properties of asphalt concretes. Transp Res Rec 1789:113–120
3. Guddati MN, Feng Z, Kim YR (2002) Towards a micromechanics-based procedure to characterize fatigue performance of asphalt concrete. Transp Res Rec 1789:121–128
4. Sadd MH, Dai Q, Parameswaran V, Shukla A (2003) Simulation of asphalt materials using a finite element micromechanical model with damage mechanics. Transp Res Rec 1832:86–95
5. Soares BJ, Freitas F, Allen DH (2003) Crack modeling of asphaltic mixtures considering heterogeneity of the material. Transp Res Rec 1832:113–120
6. Dai Q, Sadd MH, Parameswaran V, Shukla A (2005) Prediction of damage behaviors in asphalt materials using a micromechanical finite-element model and image analysis. J Eng Mech 131(7):668–677
7. Buttlar W, You Z (2001) Discrete element modeling of asphalt concrete: microfabric approach. Transp Res Rec 1757:111–118
8. Kim H, Buttler WG (2005) Micromechanical fracture modeling of hot-mix asphalt concrete based on a disk-shaped compact tension test. Electron J Assoc Asph Paving Technol 74E:209–223
9. Abbas A, Masad E, Papagiannakis T, Shenoy A (2005) Modeling of asphalt mastic stiffness using discrete elements and micromechanics analysis. Int J Pavement Eng 6(2):137–146
10. Fish J, Wagiman A (1993) Multiscale finite element method for a locally non-periodic heterogeneous medium. Comput Mech 12:164–180
11. Fish J, Belsky V (1995) Multigrid method for periodic heterogeneous media, part II: multiscale modeling and quality control in multidimensional cases. Comput Methods Appl Mech Eng 126:17–38
12. Oden JT, Zohdi TI (1997) Analysis and adaptive modeling of highly heterogeneous elastic structures. Comput Methods Appl Mech Eng 172:3–25

13. Feyel F (1999) Multiscale FE^2 elastoviscoplastic analysis of composite structures. Comput Mater Sci 16:344–354
14. Lee K, Moorthy S, Ghosh S (1999) Multiple scale computational model for damage in composite materials. Comput Methods Appl Mech Eng 172:175–201
15. Oden JT, Vemaganti K, Moes N (1999) Hierarchical modeling of heterogeneous solids. Comput Methods Appl Mech Eng 148:367–391
16. Feyel F, Chaboche JL (2000) FE^2 multiscale approach for modeling the elastoviscoplastic behavior of long fibre SiC/Ti composite materials. Comput Methods Appl Mech Eng 183:309–330
17. Fish J, Shek K (2000) Multiscale analysis of composite materials and structures. Compos Sci Technol 60:2547–2556
18. Ghosh S, Lee K, Raghavan P (2001) A multi-level computational model for multiscale damage analysis in composite and porous materials. Int J Solids Struct 38:2335–2385
19. Raghavan P, Moorthy S, Ghosh S, Pagano NJ (2001) Revisiting the composite laminate problem with an adaptive multi-level computational model. Compos Sci Technol 61:1017–1040
20. Haj-Ali RM, Muliana AH (2004) A multi-scale constitutive formulation for the nonlinear viscoelastic analysis of laminated composite materials and structures. Int J Solids Struct 41:3461–3490
21. Dugdale DS (1960) Yielding of steel sheets containing slits. J Mech Phys Solids 8:100–104
22. Barenblatt GI (1962) The mathematical theory of equilibrium cracks in brittle fracture. Adv Appl Mech 7:55–129
23. Needleman A (1987) A continuum model for void nucleation by inclusion debonding. J Appl Mech 54:525–531
24. Tvergaard V (1990) Effect of fiber debonding in a whisker-reinforced metal. Mater Sci Eng 125(2):203–213
25. Geubelle PH, Baylor J (1998) The impact-induced delamination of laminated composites: a 2D simulation. Composites B 29:589–602
26. Ortiz M, Pandolfi A (1999) Finite-deformation irreversible cohesive elements for three-dimensional crack propagation analysis. Int J Numer Methods Eng 44(9):1267–1282
27. Espinosa HD, Zavattieri PD (2003) A grain level model for the study of failure initiation and evolution in polycrystalline brittle materials. part I: theory and numerical implementation. Mech Mater 35:333–364
28. Park K, Paulino GH, Roesler JR (2009) A unified potential-based cohesive model of mixed-mode fracture. J Mech Phys Solids 57:891–908
29. Yoon C, Allen DH (1999) Damage dependent constitutive behavior and energy release rate for a cohesive zone in a thermoviscoelastic solid. Int J Fract 96:55–74
30. Allen DH, Searcy CR (2000) Numerical aspects of a micromechanical model of a cohesive zone. J Reinf Plast Compos 19(3):240–248
31. Allen DH, Searcy CR (2001) A micromechanical model for a viscoelastic cohesive zone. Int J Fract 107:159–176
32. Souza FV, Allen DH (2010) Multiscale modeling of impact on heterogeneous viscoelastic solids containing evolving microcracks. Int J Numer Methods Eng 82:464–504
33. Souza FV, Allen DH (2010) Modeling failure of heterogeneous viscoelastic solids under dynamic/impact loading due to multiple evolving cracks using a two-way coupled multiscale model. Mech Time-Dependent Mater 14(2):125–151
34. Nemat-Nasser S, Hori M (1993) Micromechanics: overall properties of heterogeneous materials. North Holland, New York
35. Allen DH (2001) Homogenization principles and their application to continuum damage mechanics. Compos Sci Technol 61:2223–2230
36. Kouznetsova VG (2002) Computational homogenization for the multi-scale analysis of multi-phase materials. PhD Dissertation, Technische Universiteit Eindhoven
37. Zocher MA, Allen DH, Groves SE (1997) A three dimensional finite element formulation for thermoviscoelastic orthotropic media. Int J Numer Methods Eng 40:2267–2288
38. Seidel GD, Allen DH, Helms KLE, Groves SE (2005) A model for predicting the evolution of damage in viscoelastic particle-reinforced composites. Mech Mater 37:163–178
39. Hill R (1967) The essential structure of constitutive laws for metal composites and polycrystals. J Mech Phys Solids 15(2):79–95
40. Souza FV (2009) Multiscale modeling of impact on heterogeneous viscoelastic solids with evolving microcracks. PhD Dissertation, University of Nebraska-Lincoln, Nebraska
41. Kim Y, Lutif JS, Allen DH (2009) Determining representative volume elements of asphalt concrete mixtures without damage. Transp Res Rec 2127:52–59
42. Kim Y, Lee J, Lutif JS (2010) Geometrical evaluation and experimental verification to determine representative volume elements of heterogeneous asphalt mixtures. J Test Eval 38(6):660–666
43. Kim Y, Aragão FTS, Allen DH, Little DN (2010) Damage modeling of bituminous mixtures through computational micromechanics and cohesive zone fracture. Can J Civ Eng 37:1125–1136
44. Aragão FTS (2011) Computational microstructure modeling of asphalt mixtures subjected to rate-dependent fracture. PhD Dissertation, University of Nebraska, Lincoln, Nebraska
45. Aragão FTS, Kim Y, Lee J, Allen DH (2011) Micromechanical model for heterogeneous asphalt concrete mixtures subjected to fracture failure. J Mater Civ Eng 23(1):30–38
46. Hugo F, Kennedy T (1985) Surface cracking of asphalt mixtures on southern africa. Proc Assoc Asph Paving Technol 54:454–496
47. Jacobs M (1995) Crack growth in asphaltic mixes. PhD Dissertation, Delft Institute of Technology, Netherlands